

# GPU-Accelerated Modified Bessel Function of the Second Kind for Gaussian Processes

Zipei Geng<sup>1</sup>, Sameh Abdulah<sup>2</sup>, Ying Sun<sup>1</sup>, Hatem Ltaief<sup>2</sup>, David E. Keyes<sup>2</sup>, Marc G. Genton<sup>1</sup>

<sup>1</sup>Statistics Program,

<sup>2</sup>Applied Mathematics and Computational Sciences (AMCS) Program,

<sup>1,2</sup>King Abdullah University of Science and Technology, Thuwal, Saudi Arabia.

<sup>1,2</sup>{firstname.lastname}@kaust.edu.sa

**Abstract**—Modified Bessel functions of the second kind are widely used in physics, engineering, spatial statistics and machine learning. Since contemporary scientific applications, including machine learning, rely on GPUs for acceleration, providing robust GPU-hosted implementations of special functions, such as the modified Bessel function, is crucial for performance. Existing implementations of the modified Bessel function of the second kind rely on CPUs and have limited coverage of the full range of values needed in some applications. In this work, we present a robust implementation of the modified Bessel function of the second kind on GPUs, eliminating the dependence on the CPU host. We cover a range of values commonly used in real applications, providing high accuracy compared to common libraries like the GNU Scientific Library (GSL) when referenced to Mathematica as the authority. Our GPU-accelerated approach also demonstrates a 2.68X performance improvement using a single A100 GPU compared to the GSL on 40-core Intel Cascade Lake CPUs. Our implementation is integrated into *ExaGeoStat*, the HPC framework for spatial data modeling, where the modified Bessel function of the second kind is required by the Matérn covariance function in generating covariance matrices. We accelerate the matrix generation process in *ExaGeoStat* by up to 12.62X with four A100 GPUs while maintaining almost the same accuracy for modeling and prediction operations using synthetic and real datasets.

**Index Terms**—Bessel function of the second kind, GPU implementation, Tile-based Matrix Computations, Gaussian processes.

## I. INTRODUCTION

The modified Bessel function of the second kind here denoted as  $K_\nu(x)$ , where  $\nu$  represents the order and  $x$  the argument, arises in a wide range of applications across mathematics, physics, engineering, spatial statistics, and machine learning. For instance, in physics and engineering,  $K_\nu(x)$  frequently appears in solving PDEs in cylindrical symmetry with radially decaying behavior. Examples include heat conduction, damped wave propagation [1], electromagnetic fields in cylindrical waveguides [2], and Schrodinger's equation in axisymmetry [3]. In machine learning, the modified Bessel function of the second kind can serve as a kernel function, mapping data into higher-dimensional spaces in algorithms such as Support Vector Machines

(SVMs) [4]. Similarly, in spatial statistics,  $K_\nu(x)$  is employed in the Matérn covariance function, which is widely used to construct correlation matrices that capture spatial relationships between locations [5]. These diverse applications emphasize the importance of efficient computation of the  $K_\nu(x)$  function.

In the literature, three methods are widely employed to compute the modified Bessel function of the second kind across a broad range of values for  $x$  and  $\nu$  [6]: series expansions [7], continued fractions [8], and asymptotic expansions [9]. The first expresses  $K_\nu(x)$  as an infinite series involving powers of  $x$ . This approach is particularly effective for small  $x$ , where truncating the series to a finite number of terms provides a highly accurate approximation. The continued fractions method represents the Bessel function as an infinite recursive fraction. This method is suitable for larger  $x$  than is the series expansion, but it remains computationally intensive. An asymptotic expansion approximates the Bessel function by capturing its dominant behavior as  $x$  becomes very large. By neglecting lower-order terms, this method efficiently describes the primary growth trend. However, it lacks accuracy for small  $x$ , where such approximations fail to converge effectively. Combining these three methods and other less common approaches can effectively cover a wider range of  $x$  and  $\nu$  values. Nevertheless, these techniques are computationally demanding and inherently sequential, posing challenges for parallelization on modern architectures, such as GPUs.

We adopt an integration-based method proposed by [6] to compute the modified Bessel function of the second kind for real order  $\nu \in \mathbb{R}$ ,  $K_\nu(x)$ , denoted by BESSELK, and optimize it for GPU implementation. This approach, implemented in CUDA, is well-suited for parallel execution, as it represents the Bessel function using quadrature over finite intervals. The key advantages of this method, beyond its parallelizability, are its flexibility and ability to efficiently cover a reasonable range of  $x$  and  $\nu$  values. Our implementation has been integrated into *ExaGeoStat* [10], a scalable geospatial data modeling and prediction framework optimized for manycore

systems, including modern GPUs.

*ExaGeoStat* possesses three functionalities: synthetic data generation, modeling, and prediction. Each of these operations requires, at a minimum, the generation of a covariance matrix of size  $N \times N$ , where  $N$  represents the number of spatial locations in its simplest form. The Matérn kernel (or covariance function), which involves the BESSELK function, is often used in Gaussian processes to construct this covariance matrix.

Our contributions are summarized as follows:

- We present a highly efficient GPU implementation of the BESSELK function, addressing a critical performance bottleneck encountered in numerous scientific applications.
- We enhance an integration-based algorithm for BESSELK to efficiently handle a reasonable range of  $x$  and  $\nu$  that is commonly encountered in spatial statistics.
- We combine the enhanced integration-based algorithm with a series expansion to accurately compute the BESSELK function for  $x < 0.1$ , where the integral-based approach specifically underperforms, making our solution more comprehensive.
- We integrate the refined algorithm into the covariance matrix generation step of *ExaGeoStat* and evaluate its performance and accuracy against existing CPU-based implementations, such as the GNU Scientific Library.
- We assess the accuracy of the proposed algorithm for computing the BESSELK function against existing approaches. Additionally, we evaluate its accuracy and overall impact within the *ExaGeoStat* software pipeline using synthetic datasets and a real-world wind speed dataset for climate and weather modeling applications.

## II. RELATED WORK

The modified Bessel function of the second kind,  $K_\nu(x)$  or BESSELK, arises in separation of variables solutions of partial differential equations [11]–[13]. A key feature of BESSELK is its *rapid decay at infinity*. The function diminishes exponentially as  $x \rightarrow \infty$ , providing a basis for solutions that vanish at large distances. Applications include heat conduction [14], wave propagation [15], and stochastic processes [16].

BESSELK also arises in the widely used Matérn kernel, a covariance function for Gaussian processes. The Matérn kernel finds extensive applications across various fields. In spatial statistics, it is employed to model spatial correlations [5]. In machine learning, it is particularly valuable for Gaussian process regression and Bayesian optimization [17]. In signal processing, it helps capture correlations in time series and spectral analysis [18].

At least six distinct methods for BESSELK can be identified in the literature; however, not all of these methods are adopted in existing tools and libraries. (1) *Series Expansions* [7]:  $K_\nu(x)$  can be expressed as an infinite series in powers of  $x$ , which is truncated to a finite number of terms when  $x$  is small. Most existing libraries utilize series expansions for small  $x$ , including MATLAB, Mathematica, GSL, SciPy, and Maple. (2) *Continued Fractions* [8]:  $K_\nu(x)$  can be represented as an infinite fraction with a recursive structure, particularly suitable when  $x$  is moderate or large. This method is also used in most existing libraries for moderate  $x$  values. (3) *Asymptotic Expansions* [9]: This method focuses on the dominant behavior of  $x$  as it becomes large, ignoring lower-order terms, which reduces accuracy for small  $x$ . This method is also used in most existing libraries for large  $x$  values. (4) *Integral Representations* [6], [20]:  $K_\nu(x)$  is expressed as integrals. This method is flexible and can work with small or large values of  $x$ . Some libraries that rely on this method include Mathematica, SciPy, and GSL. (5) *Polynomial Fitting* [21]: Polynomial fitting approximates the  $K_\nu(x)$ , by fitting polynomials to precomputed values of the function over restricted ranges of  $x$  and  $\nu$ . (6) *Differential Equation Solvers* [22]: Numerical methods for solving differential equations, such as finite difference schemes and Runge-Kutta methods [23], can be employed to compute  $K_\nu(x)$ . These solvers approximate the solution of  $K_\nu(x)$  by discretizing the domain and applying iterative algorithms to solve the governing differential equation.

## III. BACKGROUND

This section addresses the challenges in spatial statistics modeling and highlights the importance of accelerating BESSELK function computations to enhance the modeling process. Additionally, we provide an overview of the *ExaGeoStat* software and its implementation, as a testbed to evaluate our novel BESSELK implementation.

### A. Spatial Statistics and Matérn Covariance Function

Spatial statistical modeling involves analyzing and interpreting spatial data, providing insights into patterns, relationships, and dependencies within geographic or spatial domains. It also predicts missing data in a given spatial domain. A commonly used method in spatial data modeling is the maximum likelihood estimation (MLE). In MLE, an optimization process iterates over a given log-likelihood function to estimate statistical parameters that describe the underlying spatial data. This is achieved by constructing a positive definite covariance matrix that captures the correlation between different locations in the field. The log-likelihood function  $\mathcal{L}(\theta)$  is represented as:

$$\mathcal{L}(\theta) = -\frac{1}{2} [N \log(2\pi) + \log(|\Sigma(\theta)|) + \mathbf{z}^\top \Sigma(\theta)^{-1} \mathbf{z}],$$

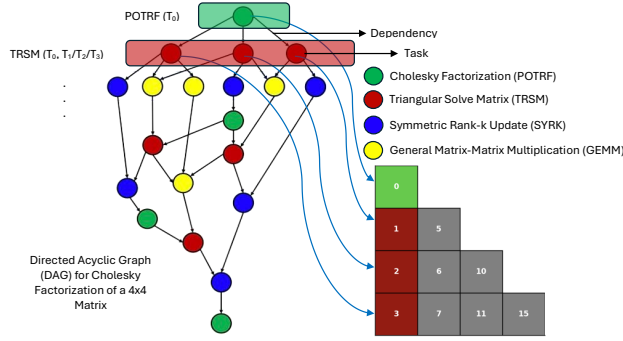


Fig. 1: Directed acyclic graph of tasks for Cholesky factorization of a  $4 \times 4$  matrix: Nodes represent tasks, edges indicate dependencies. The runtime schedules tasks to hardware while maintaining correlation constraints.

where  $\theta$  is a set of parameters to be fit,  $N$  is the number of observations,  $\Sigma(\theta)$  is the parameterized covariance matrix,  $|\Sigma(\theta)|$  is its determinant, and  $\mathbf{z}$  is the vector of observed data. The Matérn function is a widely used function in spatial statistics due to its flexibility in modeling spatial dependence [5].

The Matérn function can be represented as:

$$\mathcal{M}(r; \theta) = \frac{\sigma^2}{2^{\nu-1}\Gamma(\nu)} \left(\frac{r}{\beta}\right)^{\nu} K_{\nu}\left(\frac{r}{\beta}\right),$$

where  $r = \|\mathbf{x} - \mathbf{x}'\|$  is the distance between two spatial locations and  $\theta = (\sigma^2, \beta, \nu)^{\top}$ ,  $\nu > 0$  is a parameter that controls the smoothness of the function,  $\beta$  is the length scale parameter,  $\sigma^2$  is the variance,  $\Gamma(\nu)$  is the Gamma function, and  $K_{\nu}(\cdot)$  is the modified Bessel function of the second kind of order  $\nu$  (BESSELK( $x, \nu$ )).

The BESSELK is core in generating the covariance matrix when using the Matérn function, which is required not only during the modeling process but also for prediction tasks and the generation of synthetic datasets [24], [25].

### B. ExaGeoStat: A Parallel Tile-Based Framework for Geospatial Data Analysis

*ExaGeoStat* is a high-performance software package for large-scale climate and environmental geostatistics [10]. It evaluates the log-likelihood function for spatial datasets using a range of covariance models, including the Matérn covariance function. This enables efficient parameter estimation and prediction for large-scale spatial datasets by leveraging state-of-the-art dense linear algebra libraries (e.g., CHAMELEON [26], and DPLASMA [27]) and runtime systems (e.g., StarPU [28], and PaRSEC [29]), *ExaGeoStat* achieves high performance across diverse hardware architectures, including multicore CPUs, GPUs, and dis-

tributed systems. The software supports both exact and approximate computations [30]–[32].

*ExaGeoStat* relies on tile-based algorithms to effectively leverage the underlying runtime system for distributing tasks across available hardware resources. The runtime system efficiently schedules the processing of matrix tiles across computational units, maximizing performance and resource utilization. All executions are conducted exclusively on GPUs to further optimize the performance of *ExaGeoStat*. Figure 1 illustrates the concept of tile algorithms using the example of tile-based Cholesky factorization—a core operation in the MLE process—on a  $4 \times 4$  tiled matrix, at the stage where the (1,1) tile has been factored and its inverse action applied down the first column of tiles.

## IV. ALGORITHM FOR BESSELK

Our BESSELK algorithm is built to compute a reasonable range of  $x$ , and  $\nu$  that covers a wide spectrum of applications builds upon two existing methods: Temme’s series expansion and Takekawa’s algorithm, reviewed, respectively, in the following two subsections.

### A. Temme’s series expansion

Most existing libraries rely on series expansions to compute the BESSELK function when  $x$  is small [7]. Series expansions offer an efficient and accurate approximation in this regime, with the series expressed as:

$$K_{\nu}(x) = \sum_{k=0}^{\infty} c_k f_k, \quad K_{\nu+1}(x) = \frac{2}{x} \sum_{k=0}^{\infty} c_k h_k, \quad (1)$$

where

$$c_k = \frac{(x^2/4)^k}{k!}, \quad h_k = -k f_k + p_k,$$

and  $p_k$  and  $q_k$  are recurrence relations defined as:

$$p_k = \frac{p_{k-1}}{k - \nu}, \quad q_k = \frac{q_{k-1}}{k + \nu}.$$

The term  $f_k$  is computed iteratively:

$$f_k = \frac{k f_{k-1} + p_{k-1} + q_{k-1}}{k^2 - \nu^2}.$$

The recurrence relations are initialized with:

$$p_0 = \frac{1}{2} \left(\frac{x}{2}\right)^{-\nu} \Gamma(1+\nu), \quad q_0 = \frac{1}{2} \left(\frac{x}{2}\right)^{\nu} \Gamma(1-\nu), \quad (2)$$

$$f_0 = \frac{\nu\pi}{\sin(\nu\pi)} \left[ \cosh(\sigma)\Gamma_1(\nu) + \frac{\sinh(\sigma)}{\sigma} \ln\left(\frac{2}{x}\right)\Gamma_2(\nu) \right], \quad (3)$$

where  $\sigma$  and  $\Gamma_1(\nu)$ ,  $\Gamma_2(\nu)$  are precomputed constants for the expansion.

The original formulation of Temme’s series expansion in [7] does not provide sufficiently stable or accurate results for  $\nu \geq 1.5$ . Direct evaluation of  $p_0, q_0$ , and  $f_0$

for large orders of  $\nu$  increases the error of this approximation method. To address these limitations and improve numerical stability and accuracy, Campbell [34] proposed leveraging the recurrence relation for large-order  $\nu = \mu + M$  (where  $M = \lfloor \nu + 0.5 \rfloor$ ) of  $K_\nu(x)$ .

This approach uses starting values  $K_\mu(x)$  and  $K_{\mu+1}(x)$ , with  $-\frac{1}{2} \leq \mu < \frac{1}{2}$ , and applies the forward recurrence relation:

$$K_{\eta+1}(x) = \left(\frac{2\eta}{x}\right) K_\eta(x) + K_{\eta-1}(x). \quad (4)$$

We employ Temme's series expansion and the recurrence relation to evaluate the BESSELK function in the small- $x$  regime ( $x < 0.1$ ).

### B. Integral-based Algorithm (Takekawa's Approach)

In [6], Takekawa introduced a method to compute the BESSELK function using an integral approach.  $K_\nu(x)$ , is represented by the following integral form [35]:

$$K_\nu(x) = \int_0^\infty e^{-x \cosh(t)} \cosh(\nu t) dt \quad (5)$$

where  $x > 0$  and  $\nu \in \mathbb{R}$ . This representation is computationally intensive but provides accurate results, especially for small and moderate  $x$ .

Takekawa worked with the logarithm of the integrand

$$e^{-x \cosh(t)} \cosh(\nu t) \quad (6)$$

namely,

$$g_{\nu,x}(t) = \log \cosh(\nu t) - x \cosh(t). \quad (7)$$

The first-order, and second-order derivatives of  $g_{\nu,x}(t)$  with respect to  $t$  are given by:

$$\begin{aligned} g'_{\nu,x}(t) &= \nu \tanh(\nu t) - x \sinh(t), \\ g''_{\nu,x}(t) &= \nu^2 \operatorname{sech}^2(\nu t) - x \cosh(t). \end{aligned}$$

At  $t = 0$ , we have  $g_{\nu,x}(0) = -x$  and  $g'_{\nu,x}(0) = 0$ . Consequently, if  $\nu^2 \leq x$ , the function  $g_{\nu,x}(t)$  will always decrease, implying that the maximum value of the function in Equation (6) occurs at  $t = 0$ , as  $g''_{\nu,x}(0) \leq 0$ . In contrast, if  $\nu^2 > x$ , the function in Equation (6) will reach its maximum at some  $t \geq 0$ , since  $g''_{\nu,x}(0) > 0$ . Further details are provided in [6].

To integrate Equation (6), the region where the maximum value of  $t$ , denoted as  $t_{\max}$ , is located, can be defined as the region where  $g_{\nu,x}(t) \leq \epsilon_{\text{machine}} \times g_{\nu,x}(t_{\max})$ . Here,  $\epsilon_{\text{machine}} = \min\{\epsilon > 0 \mid 1 + \epsilon \neq 1\}$ . This region can be expressed as a single continuous interval  $[t_0, t_1]$ , defined as:

$$[t_0, t_1] = \{t \mid g_{\nu,x}(t) \geq g_{\nu,x}(t_{\max}) + \log(\epsilon_{\text{machine}})\}. \quad (8)$$

Takekawa defines the integral range by determining  $t_{\max}$  from Equation (7). If  $\nu^2 \leq x$ , then  $t_{\max} = 0$ . Otherwise,  $t_{\max}$  can be found by searching within a specific

range of the function  $g_{\nu,x}(t)$ . Since  $g'_{\nu,x}(t_{\max}) = 0$ , the range can be defined as  $[2^m, 2^{m+1}]$ , where  $m$  is the smallest value such that  $g'_{\nu,x}(2^m) < 0$ . For a detailed explanation, refer to the *FINDRANGE* algorithm in [6]. Afterwards, the  $t_{\max}$  value can be obtained using binary search and Newton methods, refer to the *FINDZERO* algorithm in [6].

The integration range is also determined using the *FINDZERO* algorithm. To compute  $t_0$  (the lower bound of integration), if  $\nu^2 \leq x$ , then  $t_0 = 0$ . Otherwise, the *FINDZERO* algorithm is applied to find  $t_0$  within the range  $[t_0, t_{\max}]$ . For  $t_1$ , the *FINDZERO* algorithm is similarly employed to search within the range  $[t_{\max} + 2^{m+1}, t_{\max} + 2^m]$ .

After determining  $t_0$  and  $t_1$ , integration is performed over the range using a fixed number of number of bins  $= b$ . To ensure numerical stability, the `log_sum_exp` function is applied to  $g_{\nu,x}(t_m)$ , resulting in:

$$\begin{aligned} \log K_\nu(x) &\approx g_{\nu,x}(t_{\max}) + \\ &\log \sum_{m=0}^b h \exp \left\{ c_m (g_{\nu,x}(t_m) - g_{\nu,x}(t_{\max})) \right\}. \end{aligned} \quad (9)$$

Here, the parameters are defined as:

$$h = \frac{t_1 - t_0}{b}, \quad t_m = t_0 + mh,$$

$$c_0 = c_n = \frac{1}{2}, \quad c_m = 1 \quad (m = 1, \dots, b-1).$$

Finally, the value of  $K_\nu(x)$  can be obtained by taking the exponential.

### C. The Proposed Refined Algorithm

Existing numerical libraries, such as MATLAB, SciPy, and Boost C++, offer no GPU support for evaluating the BESSELK function, resulting in a significant performance bottleneck for GPU-accelerated scientific applications that depend on this function. Performing BESSELK computations on the CPU while executing other tasks on the GPU is highly time-consuming due to the overhead of data transfers between the CPU and GPU and the GPU's superior parallel processing capabilities compared to the CPU.

While Plesner et al. [33] recently introduced a GPU-accelerated library for BESSELK evaluation, its performance gains are limited. Their implementation outperforms GSL only within the parameter range  $(x, \nu) \in (150, 4000] \times (150, 4000]$  and exhibits largely limited performance outside this range compared to GSL.

To address this gap, we propose a novel approach that advances the state-of-the-art in GPU-accelerated BESSELK computation, delivering improved performance across a reasonable parameter space. We adopt the quadrature-based algorithm proposed by

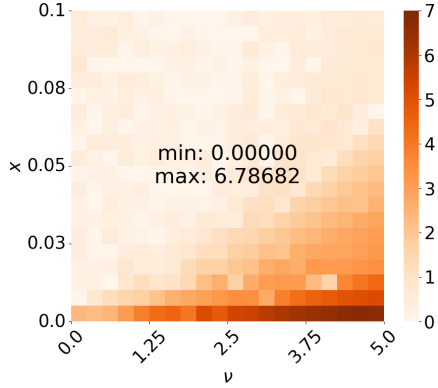


Fig. 2: Relative error of Takekawa’s algorithm vs. Mathematica for  $(\nu, x) \in [0.001, 5] \times [0.001, 0.1]$ .

Takekawa [6]. Although Takekawa’s algorithm demonstrates substantial accuracy for large values of  $x$  and  $\nu$ , it notably lacks discussion of cases where  $x < 0.1$ —a range frequently encountered in applications such as spatial statistics. Our analysis reveals that within this range, the integration algorithm exhibits a significant loss of accuracy. Figure 2 shows a heatmap of the relative error in Takekawa’s approach for  $x < 0.1$ , compared to referential results obtained using Mathematica [36]. Following Takekawa in [6], we compute the relative error (RE) at each  $x$  and  $\nu$  as:

$$\text{RE} = \log_{10} \left( 1 + \frac{|\text{Mathematica's output} - \text{output}|}{\varepsilon_{\text{machine}}} \right)$$

where  $\varepsilon_{\text{machine}}$  is the machine epsilon, and  $\varepsilon_{\text{machine}} = 2^{-52} \approx 2.22 \times 10^{-16}$  for double-precision numbers.

We propose a novel algorithm for the BESSELK function that extends the range of  $x$  values beyond those supported by Takekawa’s method. We refer to this enhanced approach as the *Refined Algorithm*. Furthermore, we provide an efficient GPU-based implementation for generating large matrices using BESSELK within the *ExaGeoStat* software relying on the *StarPU* runtime system. Our key contributions to improving Takekawa’s algorithm are summarized as follows:

- Our algorithm sets the lower bound of the integral in Equation (5) to 0 instead of explicitly calculating it. We observed that reducing the integral range by computing  $t_0$  and  $t_1$  is more computationally expensive than extending the integral range on the GPU.
- The refined algorithm sets the upper bound of the integral to the maximum value determined through our empirical analysis (discussed later) on Mathematica, ensuring it is applicable across all ranges of  $x$  and  $\nu$  encountered in various applications.
- Instead of searching for a global  $t_{\text{max}}$  using the *FINDZERO* algorithm, as done in Takekawa’s al-

gorithm, we compute a local  $t_{\text{max}}$  for each division (two divisions form a bin) within the integral range. This localized approach enables faster computation compared to identifying a global maximum.

- We increase the number of bins  $b$  in the integral because of expanding the integral range  $[t_0, t_1]$ . This enhancement significantly improves the accuracy of the Bessel function in many cases while having minimal impact on performance due to the computational power of GPUs.
- To address the high error in Takekawa’s method for  $x < 0.1$ , we combine the integral algorithm with Temme’s expansion. This refinement reduces the relative error from 6.78682 in Takekawa’s algorithm to 0.73180 in the refined algorithm for this range, given a sufficient number of bins.

---

#### Algorithm 1 Empirical Upper Bound Finding

---

- 1: **Given:**  $\mathcal{X} \times \mathcal{V} = [0, 140] \times (0, 20]$ , MBK( $x, \nu$ ) the reference level of LOGBESSELK using Mathematica, and  $\text{RBK}(x, \nu) := \log \left[ \int_0^L e^{-x \cosh(t)} \cosh(\nu t) dt \right]$ , where the integration follows the Equation (9).
  - 2: **for all**  $(x, \nu) \in \mathcal{X} \times \mathcal{V}$  **do**
  - 3:     AE( $x, \nu$ )  $\leftarrow$   $|\text{MBK}(x, \nu) - \text{RBK}(x, \nu)|$  (Absolute Error for ( $x, \nu$ ))
  - 4:  $t_1 \leftarrow \min L$  s.t.  $\max_{x, \nu} \text{AE}(x, \nu) \leq 10^{-9}$
- 

For  $x \in [0.1, \infty)$ , we use a refined version of the integration algorithm proposed in [6] to evaluate BESSELK. Instead of determining the integration range  $[t_0, t_1]$  dynamically based on  $x$  and  $\nu$ , we fix  $t_0 = 0$  and  $t_1 = 9$ . We set  $t_0 = 0$  to match the integral’s starting point, and through empirical tests, we establish  $t_1 = 9$  as the optimal endpoint for parameters within  $(x, \nu) \in [0, 140] \times (0, 20]$ , which corresponds to the expected parameter range in geospatial applications involving the Matérn kernel. The process for empirically finding the upper bound is outlined in Algorithm 1. This broader integration range may slightly increase computational cost but improves GPU efficiency by avoiding performance-degrading conditional branching.

Algorithm 2 provides a detailed explanation of the steps of our proposed algorithm. The inputs are the pair  $(x, \nu)$  to compute  $K_\nu(x)$ . To define  $b$  the number of bins, increasing the number of bins can improve accuracy, but at the cost of reduced performance, as the algorithm must identify the local maximum point  $t_{\text{max}}$  for each division. However, we observed that fixing the number of bins to 40 provides a balance, achieving an accuracy threshold that ensures computational stability across different values of  $x$  and  $\nu$ . In Algorithm 2, Temme’s expansion method is used to compute the Bessel function if  $x \leq 0.1$  (lines 3-7); otherwise, use Equation 9 to compute the Bessel function using  $b$  bins (lines 8-13).

**Algorithm 2** Refined Algorithm (BESSELK( $x, \nu$ ))

---

```

1: Input:  $(x, \nu) \in \mathcal{X} \times \mathcal{V}$ , where  $\mathcal{X} \times \mathcal{V}$  is the problem
   region of evaluation of BESSELK
2: Given:  $b$  number of bins for numerical integration
3: if  $0 \leq x < 0.1$  and  $\nu \in \mathcal{V}$  then
4:   Set  $M = \lfloor \nu + 0.5 \rfloor$  and use  $\mu = \nu - M$ 
5:   Use Equation (2) and Equation (3) to initialize
    $p_0, q_0, f_0$  for smoothness  $\mu$ 
6:   Set 15000 instead of  $\infty$  for the sum of Temme's series
   for  $K_\mu(x)$  in Equation (1)
7:   Use the recurrence relation
   
$$K_{\eta+1}(x) = \left(\frac{2\eta}{x}\right) K_\eta(x) + K_{\eta-1}(x)$$

   until  $\eta + 1 = \nu$  to acquire  $K_\nu(x)$ 
8: else  $x \in \mathcal{X} \setminus [0, 0.1)$  and  $\nu \in \mathcal{V}$ 
9:    $t_0 \leftarrow$  LB (fixed to 0)
10:   $t_1 \leftarrow$  UB (empirical upper bound for all  $(x, \nu)$ )
11:   $t_{\max} \leftarrow \max_{i=0, \dots, b} t_i$ 
12:  Use
   
$$\log K_\nu(x) \leftarrow g_{\nu, x}(t_{\max}) +$$

   
$$\log \sum_{m=0}^b h \exp \left\{ c_m (g_{\nu, x}(t_m) - g_{\nu, x}(t_{\max})) \right\},$$

   where  $h, t_m, c_m$  are given in Equation (9) and  $g_{\nu, x}(\cdot)$ 
   given in Equation (7)
13:   $K_\nu(x) \leftarrow \exp(\log(K_\nu(x)))$ 
14: Output:  $\text{BESSELK}(x, \nu) \leftarrow K_\nu(x)$ 

```

---

Algorithm 3 presents the pseudocode for the CUDA algorithm used to generate a single tile of the covariance matrix based on the Matérn covariance function and the BESSELK function, leveraging the refined algorithm. Using the *StarPU* runtime scheduler, each tile is assigned to a different GPU to compute the full covariance matrix. Memory allocation is handled via `starpu_malloc()` to optimize data transfer performance between the CPU (host) and the GPU. In lines 5-13, each GPU thread processes a single tile value to compute the BESSELK function based on the corresponding  $x$  value, as described in Algorithm 2.

## V. EXPERIMENTAL RESULTS

In this section, we evaluate the implementation of the refined BESSELK algorithm on the GPU within the *ExaGeoStat* software, focusing on its impact in accelerating the computation of individual matrix elements when millions to trillions of elements are computed. The experiments focus on four main objectives: (1) Assessing the accuracy of computing the modified Bessel function of the second kind for specific  $x$  and  $\nu$  values. (2) Analyzing the overall accuracy of spatial statistical modeling using a synthetic dataset, with emphasis on our GPU-based implementation for matrix generation across different spatial correlation levels. (3) Validating the

**Algorithm 3** GPU Single-Tile Matérn Covariance Generation Algorithm

---

```

1: function GENERATEMATÉRNCOVARIANCE( $\ell_x^1, \ell_y^1, \ell_x^2, \ell_y^2,$ 
    $\sigma, \beta, \nu, m, n$ ) where  $\ell^1$  and  $\ell^2$  represents location vectors.
2:   Initialize CUDA grid with dimension  $(m+8-1//m) *$ 
    $(n+8-1//n)$  and block dimensions  $8 \times 8$  (which
   means 64 threads for each block)
3:   Use starpu_malloc() for efficient CUDA mem-
   ory allocation, enabling fast CPU-GPU and GPU-GPU
   transfers.
4:   Copy location vectors and parameters to GPU memory
5:   for each thread  $(i, j)$  in parallel do
6:     if  $i < m$  and  $j < n$  then
7:        $c \leftarrow \sigma^2 / (2^{\nu-1} \Gamma(\nu))$ 
8:        $d \leftarrow \sqrt{(\ell_x^2[j] - \ell_x^1[i])^2 + (\ell_y^2[j] - \ell_y^1[i])^2}$ 
9:        $r \leftarrow d/\beta$ 
10:      if  $r = 0$  then
11:         $A[i + j \times m] \leftarrow \sigma^2$ 
12:      else
13:         $A[i + j \times m] \leftarrow c \cdot r^\nu \cdot \text{BESSELK}(r, \nu)$ 
14:   Transfer back the generated submatrices and param-
   eters to CPU
15:   Synchronize CUDA stream
16: Free the CUDA memory and destroy the CUDA stream

```

---

accuracy of the proposed implementation in modeling real datasets within the context of climate and weather applications. (4) Evaluating the performance of full covariance matrix generation within *ExaGeoStat*, using both single and multiple GPUs.

## A. Relative Error Analysis Against Mathematica

For accuracy assessment, existing work on implementing the BESSELK function often uses Mathematica's `BesselK[ $\nu, x$ ]` as the benchmark. In this study, we compare the performance of the GSL library, Takekawa's algorithm, and the refined algorithm against Mathematica. The relative errors for various values of  $x$  and  $\nu$  are presented as a heatmap. The heatmap spans the region  $(\nu, x) \in [0.001, 20] \times [0.001, 140]$ , which adequately covers the parameter range relevant to spatial statistics.

Figure 3 presents three heatmaps for the target region using the three implementations. As shown, the relative errors of the LOGBESSELK in Takekawa's algorithm are larger than those of GSL and the refined algorithm, with a maximum error of 6.54807. This is primarily due to the uncovered region where  $x < 0.1$ . GSL and the refined algorithm exhibit very close relative errors, with values of 1.67896 and 1.65466, respectively. To highlight the advantages of our method over Takekawa's method for  $x \leq 0.1$ , we further zoom into the region  $(\nu, x) \in [0.001, 5] \times [0.001, 0.1]$  in Figure 4.

## B. Spatial Data Modeling Accuracy within ExaGeoStat

Estimating the relative error of the Bessel function for each pair  $(x, \nu)$  is crucial to evaluating the effectiveness of a given implementation. Beyond this, however, the

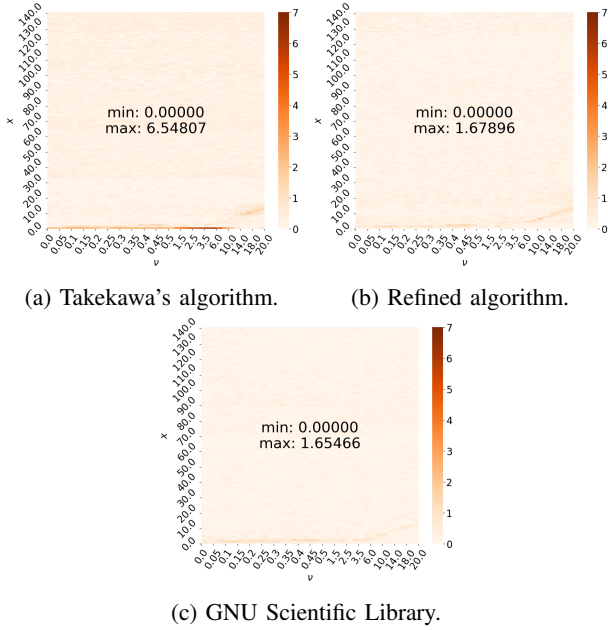


Fig. 3: LOGBESSELK accuracy comparisons using heatmap for  $(\nu, x) \in [0.001, 20] \times [0.001, 140]$ .

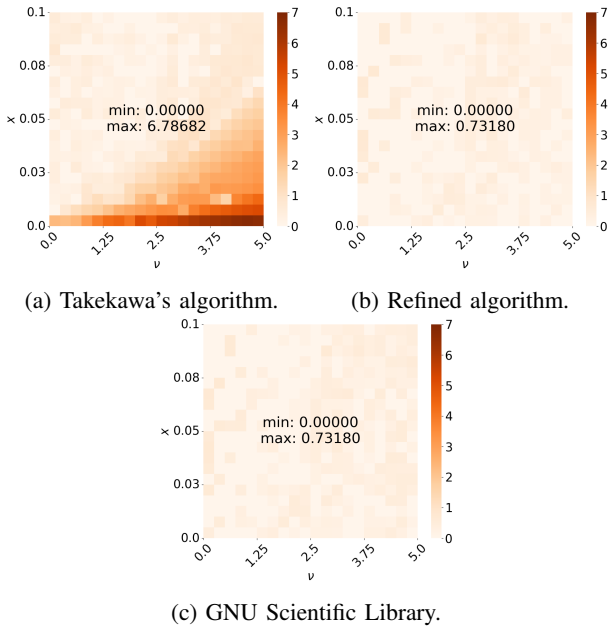


Fig. 4: LOGBESSELK accuracy comparisons using heatmap for  $(\nu, x) \in [0.001, 5] \times [0.001, 0.1]$ .

modified Bessel function, which is buried within a kernel to generate a full matrix, can affect the accuracy of subsequent matrix operations if the accumulated error from different calculations becomes significant. To assess this point, we integrate our implementation into *ExaGeoStat* to generate a full covariance matrix using

the Matérn kernel for many values in parallel. We use the spatial modeling process in *ExaGeoStat*, specifically the maximum likelihood estimate (MLE) with gradient-free optimization, which requires multiple iterations to converge and generate a set of estimated parameters  $\sigma^2$ ,  $\beta$ , and  $\nu$  that effectively describe the underlying spatial domain.

The accuracy of the MLE operation is typically evaluated using Monte Carlo simulations in which synthetic spatial data are generated [37]. In the simplest case, this involves  $(x, y, z)$ , where  $(x, y)$  represents spatial locations, and  $z$  denotes the measurement value at  $(x, y)$ . We use synthetic data generated at irregular locations within a two-dimensional space, as described in [38]. We evaluated the accuracy of the modeling results across three representative scenarios commonly encountered in spatial statistics. These scenarios were characterized by different levels of spatial correlation: weak ( $\sigma^2 = 1, \beta = 0.03, \nu = 0.5$ ), medium ( $\sigma^2 = 1, \beta = 0.1, \nu = 0.5$ ), and strong ( $\sigma^2 = 1, \beta = 0.3, \nu = 0.5$ ).

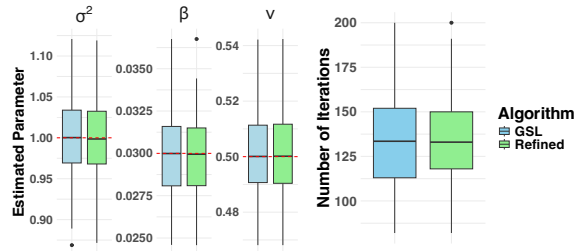
Figure 5 provides a comparison of parameter estimation using MLE, leveraging both GSL and the proposed refined algorithm. The analysis, conducted across three correlation levels (weak, medium, and strong), includes boxplots illustrating the estimation of three key parameters ( $\sigma^2$ ,  $\beta$ , and  $\nu$ ), iteration counts, and log-likelihood values.

In the weak correlation scenario (Figure 5a), both implementations achieve comparable accuracy in parameter estimation. However, the refined algorithm demonstrates slightly tighter distributions for all parameters than GSL. Additionally, the average iteration count for the refined algorithm is similar to that of GSL, indicating comparable computational efficiency. The medium correlation scenario (Figure 5b) demonstrates increased variability in parameter estimation, particularly for the  $\sigma^2$  parameter. Both implementations maintain comparable accuracy, but the refined algorithm exhibits slightly more consistent estimates across all parameters. The iteration counts remain similar.

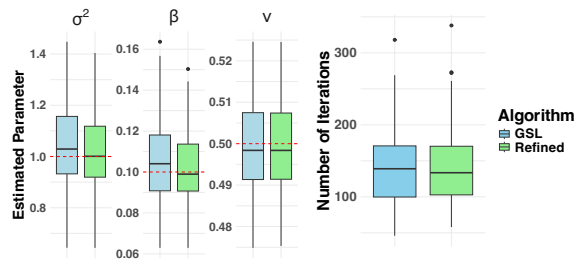
For strong spatial correlation (Figure 5c), the most challenging scenario, both implementations exhibit wider parameter distributions, reflecting the increased complexity of the estimation process. The refined algorithm achieves comparable accuracy while requiring slightly more iterations (average = 157.34) than the CPU implementation (average = 149.24).

These results indicate that the refined algorithm preserves the statistical accuracy of the traditional CPU-based GSL library while achieving improved computational efficiency. Despite requiring a similar number of optimization iterations, each iteration is significantly faster, as demonstrated in the next section. Furthermore, the consistent performance across varying correlation

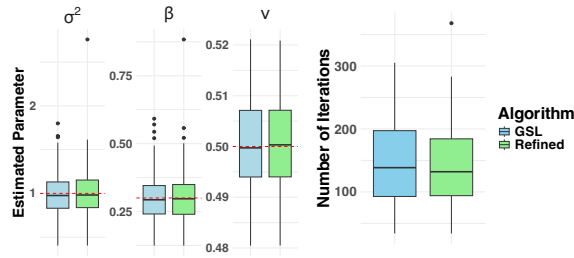
strengths highlights the robustness of the refined algorithm for spatial statistics applications.



(a) Weak correlation  $\beta = 0.03$ .



(b) Medium correlation  $\beta = 0.1$ .



(c) Strong correlation  $\beta = 0.3$ .

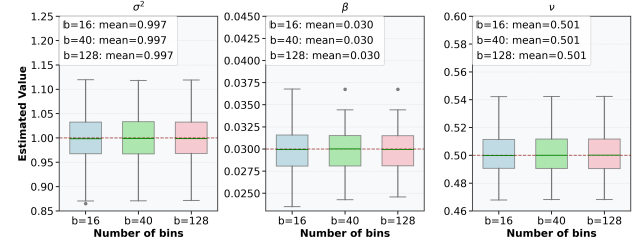
Fig. 5: Boxplots of MLE optimization results over 100 replicas using GSL on CPU and the refined algorithm on GPU, comparing estimated parameters ( $\sigma^2$ ,  $\beta$ ,  $\nu$ ) and iteration counts.

### C. Accuracy Across Different Numbers of Bins

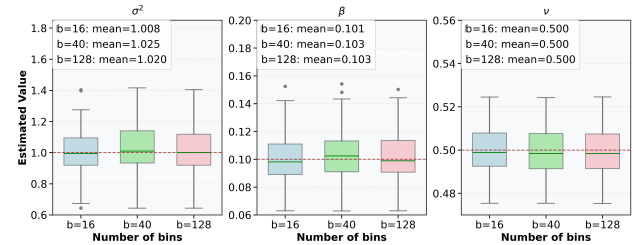
The numerical approximation accuracy of the BESSELK function, as defined in Equation (9), is significantly influenced by the discretization parameter  $b$  (number of bins). Herein, we vary the number of bins ( $b = 16, 40$ , and  $128$ ) to assess its impact on the estimated parameters under weak, medium, and strong correlation levels, as illustrated in Figure 6. Additionally, we analyze the effect of the number of bins on the iteration count required for convergence across the three correlation levels, as shown in Figure 7.

While a smaller number of bins might introduce larger approximation errors given fixed integration bounds, this does not significantly impact the MLE procedure.

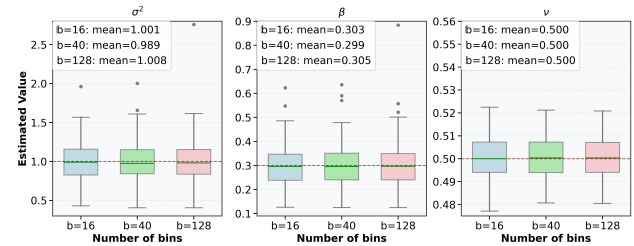
This assertion is supported by MLE algorithms typically employing convergence tolerances  $10^{-7}$ . Therefore, the choice of bin count plays a less critical role in the overall MLE parameter estimation than expected. Our approach suggests a practical balance between computational efficiency and numerical accuracy in evaluating the Matérn covariance function. Through extensive numerical experiments (Figures 6 and 7), we have empirically demonstrated that parameter estimation remains robust even with a reduced number of bins, supporting our hypothesis that accurate estimation can be achieved without requiring fine-grained discretization.



(a) Weak correlation  $\beta = 0.03$ .



(b) Medium correlation  $\beta = 0.1$ .



(c) Strong correlation  $\beta = 0.3$ .

Fig. 6: Parameter estimation over 100 replicas using the refined algorithm was evaluated for varying bin counts to estimate  $\sigma^2$ ,  $\beta$ , and  $\nu$  across different correlation levels with problem size 51,076.

### D. Wind Speed Application

For the real data analysis in this study, we use wind speed dataset of 1M locations generated using the WRF-ARW model for the Arabian Peninsula. The model features a horizontal grid resolution of 5 km and 51 vertical levels, extending to a maximum altitude of 10 hPa. The dataset spans a geographical region



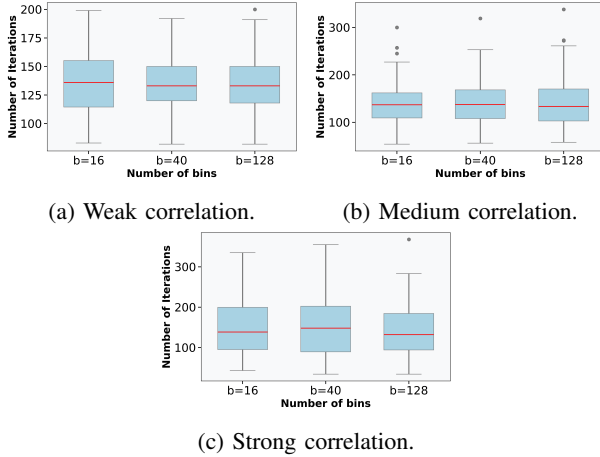


Fig. 7: The number of iterations for MLE optimization over 100 replicas using the refined algorithm was evaluated with  $b = 16, 40,$  and  $128$  bins across different correlation levels with problem size  $51,076$ .

from  $20^\circ\text{E}$  to  $83^\circ\text{E}$  longitude and  $5^\circ\text{S}$  to  $36^\circ\text{N}$  latitude, covering 37 years of daily records. Each file contains hourly wind speed measurements across 17 atmospheric layers. Our analysis specifically focused on wind speed data from September 1, 2017, at 00:00 AM, examining measurements at 10 meters above ground level (layer 0). To address the skewed distribution of wind speeds, we plotted the square root of wind speed against longitude and latitude, as shown in Figure 8.

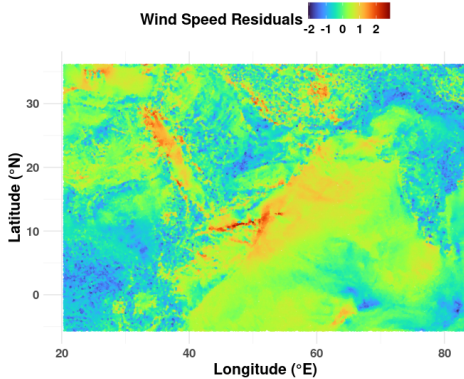


Fig. 8: Residuals of a wind speed dataset of 1M locations in the Middle East region.

Starting with an initial dataset of 1M locations, we randomly sampled 160,000 locations for modeling and 25,000 for testing. To improve numerical stability, the location coordinates are preprocessed through normalization. Given the length and width of a squared region  $\ell_1, \ell_2$ : (1) Compute the scaling factor  $\ell := \max(\ell_1, \ell_2)$ . (2) Rescale location  $(x_0, y_0)$  to  $(\{x_0 - \min(x_0)\}/\ell, \{y_0 - \min(y_0)\}/\ell)$ . This transformation maps the spatial co-

ordinates into a unit square  $[0, 1] \times [0, 1]$ , which helps mitigate numerical issues in subsequent computations.

Table I presents the estimated parameters and the final log-likelihood values obtained by the GSL and refined algorithms. The experiments were conducted on a 40-core Intel Cascade Lake CPU with 383GB memory and a single A100 GPU with 80GB memory. Both methods estimated nearly identical parameters, achieved nearly the same maximum log-likelihood value (llh), and produced the same mean square prediction error (MSPE).

However, using the GSL library required 596.61 minutes of execution time, while the refined algorithm reduced this to 299.89 minutes. For fairness, only the matrix generation was performed either by the CPU (GSL) or the GPU (refined algorithm), while all other operations were executed on the GPU.

	$(\sigma^2, \beta, \nu)$	llh	MSPE	Time (min)
GSL	(2.505, 0.178, 0.426)	6984.660	0.037188	596.61
Refined	(2.510, 0.179, 0.426)	6984.598	0.037186	299.89

TABLE I: Comparison of GSL and refined algorithms on 160K random locations from the wind speed dataset.

### E. Performance Assessment

For single-node performance evaluation, we use a 40-core Intel Cascade Lake CPU to run the GSL version and generate an entire covariance matrix within the *ExaGeoStat* framework for varying numbers of locations. Additionally, we use 1 to 4 V100 (32 GB) or A100 (80 GB) GPUs on a single node to evaluate the implementation of the refined algorithm.

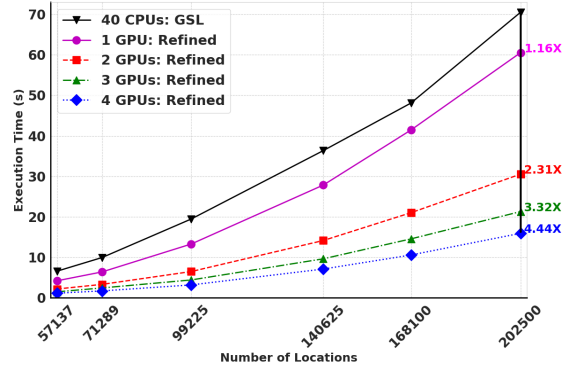


Fig. 9: Mean execution time (s) for generating an  $N \times N$  covariance matrix using GSL and the refined algorithm on a 40-core Intel Cascade Lake CPU and 1-4 NVIDIA V100 GPUs.

In the single-GPU (V100) configuration (Figure 9), tests on datasets with locations ranging from 57,137 to 202,500 demonstrated that the refined algorithm

achieved a 1.16X speedup compared to the CPU-only implementation. The performance improvements became increasingly pronounced with additional GPUs, reaching a 4.44X speedup with four GPUs. For NVIDIA A100 GPUs, the single-GPU configuration (Figure 10), tested on datasets with locations ranging from 57,137 to 99,225, showed a 2.68X speedup over the CPU-only implementation. This improvement scaled significantly with additional GPUs, achieving a 12.62X speedup with four GPUs. These results highlight the effectiveness of GPU acceleration with the refined algorithm for matrix generation, with benefits becoming more pronounced when leveraging multiple GPUs and larger datasets.

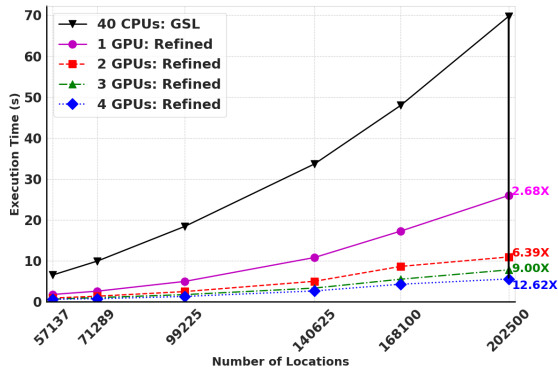


Fig. 10: Mean execution time (s) for generating an  $N \times N$  covariance matrix using GSL and the refined algorithm on a 40-core Intel Cascade Lake CPU and 1-4 NVIDIA A100 GPUs.

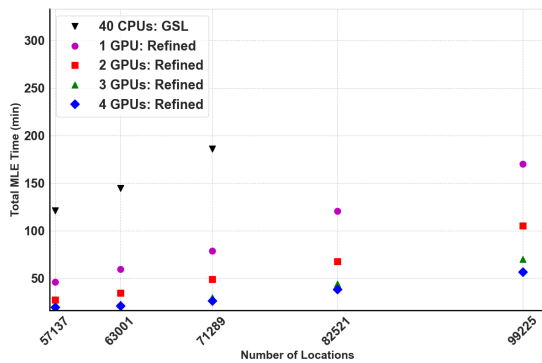


Fig. 11: Comparison of overall MLE execution time between the GSL library and the refined algorithm on a V100 GPU across various problem sizes. The reported time accounts for multiple iterations of the log-likelihood function, including matrix generation and all associated linear algebra operations within the MLE process [10].

Although the single matrix generation time highlights the efficiency of the refined algorithm on GPUs compared to GSL, its impact becomes even more signifi-

cant in operations like Maximum Likelihood Estimation (MLE). During MLE, the matrix generation function is invoked multiple times while optimizing the log-likelihood function until convergence, amplifying the benefits of the refined algorithm. Figure 11 illustrates the performance of executing the full MLE process on five different problem sizes, comparing the GSL implementation with the refined algorithm using up to four A100 GPUs. Due to the long execution time of the GSL function, the full MLE process was not estimated for  $N = 82,521$  and  $N = 99,225$ . For  $N = 71,289$ , the complete MLE process took 186.21 minutes with GSL (CPU) and 78.87, 49.36, 30.01, and 26.38 minutes using the refined algorithm on 1 GPU, 2 GPUs, 3 GPUs, and 4 GPUs, respectively.

Figure 12 also shows the scalability of the refined algorithm across up to 6 nodes, each equipped with two V100/A100 GPUs. As available memory increases, GPUs can handle larger problem sizes, and the performance scales almost linearly with adding more GPUs.

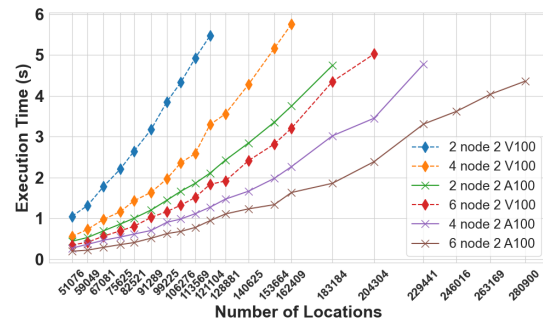


Fig. 12: Mean matrix generation time varying node counts and GPU architectures (V100 and A100).

## VI. CONCLUSION

We present a highly efficient GPU-accelerated implementation of the modified Bessel function of the second kind (BESSELK) using CUDA, effectively addressing critical computational bottlenecks in spatial statistics and various other scientific applications. The proposed method integrates Temme's series expansion for small input values and a refined version of Takekawa's integral-based approach for larger values, ensuring accuracy and computational efficiency across a reasonable parameter space. Incorporating this optimized algorithm into the *ExaGeoStat* framework demonstrates significant performance improvements in generating covariance matrices for spatial data modeling. The GPU-based implementation achieved substantial speedups compared to traditional CPU-based methods while maintaining high numerical accuracy, validated through synthetic datasets and real-world climate data. These improvements are

particularly notable in large-scale applications requiring massive matrix computations. Our work enhances the computational capabilities of BESSELK evaluations on GPUs and sets a foundation for integrating such optimizations into other domains reliant on these functions. Future directions include extending this framework to higher-dimensional spatial models and implementing derivatives of BesselK to support gradient-based optimization techniques.

## REFERENCES

- [1] Sharma, Kal Renganathan, "Damped wave conduction and relaxation in cylindrical and spherical coordinates," *Journal of Thermophysics and Heat Transfer*, vol. 21, no. 4, pp. 688–693, 2007.
- [2] Karamian, Asghar, Jazi, Bahram, and Najari, Samaneh, "The Role of Ordinary Bessel and Hankel Functions in Simulation of Plasma Valve Mechanism in a Loss-Free Metallic Cylindrical Waveguide," *Mathematics Interdisciplinary Research*, vol. 7, no. 4, pp. 343–355, 2022, University of Kashan.
- [3] Martín, Pablo, Rojas, Eduardo, Olivares, Jorge, and Sotomayor, Adrián, "Quasi-Rational Analytic Approximation for the Modified Bessel Function  $I_1(x)$  with High Accuracy," *Symmetry*, vol. 13, no. 5, p. 741, 2021, MDPI.
- [4] Ramakrishnan, Rahul O. and Friedrich, Benjamin M., "Learning run-and-tumble chemotaxis with support vector machines," *Europhysics Letters*, vol. 142, no. 4, p. 47001, 2023, IOP Publishing.
- [5] Wang, Kesen, Abdulah, Sameh, Sun, Ying, and Genton, Marc G., "Which parameterization of the Matérn covariance function?," *Spatial Statistics*, vol. 58, p. 100787, 2023, Elsevier.
- [6] Takekawa, T., 2022. Fast parallel calculation of modified Bessel function of the second kind and its derivatives. *SoftwareX*, 17, p.100923.
- [7] Temme, N.M., 1975. On the numerical evaluation of the modified Bessel function of the third kind. *Journal of Computational Physics*, 19(3), pp.324-337.
- [8] Amos, Donald E., "Computation of modified Bessel functions and their ratios," *Mathematics of Computation*, vol. 28, no. 125, pp. 239–251, 1974.
- [9] F.W.J. Olver and L.C. Maximon, "Bessel Functions," in *NIST Handbook of Mathematical Functions*, Cambridge University Press, 2009, pp. 215–286.
- [10] S. Abdulah, H. Ltaief, Y. Sun, M. G. Genton, and D. E. Keyes, "ExaGeoStat: A high performance unified software for geostatistics on manycore systems," *IEEE Transactions on Parallel and Distributed Systems*, vol. 29, no. 12, pp. 2771–2784, 2018.
- [11] Weisstein, Eric W., "Modified Bessel Function of the Second Kind," *MathWorld – A Wolfram Web Resource*, Wolfram Research, Inc., 2002. Available at: <https://mathworld.wolfram.com/>.
- [12] Dunster, T. Mark, "Bessel Functions of Purely Imaginary Order, with an Application to Second-Order Linear Differential Equations Having a Large Parameter," *SIAM Journal on Mathematical Analysis*, vol. 21, no. 4, 1990, pp. 995–1018, SIAM.
- [13] Zhukovsky, K. V., "Solving Evolutionary-Type Differential Equations and Physical Problems Using the Operator Method," *Theoretical and Mathematical Physics*, vol. 190, 2017, pp. 52–68, Springer.
- [14] Hetnarski, Richard B., and Eslami, M. Reza, "Heat Conduction Problems," *Thermal Stresses—Advanced Theory and Applications*, Springer, 2009, pp. 132–218.
- [15] Gómez-Corraea, J. E., Balderas-Mata, S. E., Coello, V., Puente, N. P., Rogel-Salazar, J., and Chávez-Cerda, S., "On the Physics of Propagating Bessel Modes in Cylindrical Waveguides," *American Journal of Physics*, vol. 85, no. 5, 2017, pp. 341–345, AIP Publishing.
- [16] Pogány, Tibor K., "Bessel–Sampling Restoration of Stochastic Signals," *Acta Polytechnica Hungarica*, vol. 10, no. 7, 2013, pp. 7–19.
- [17] AlBahar, Areej, Kim, Inyoung, and Yue, Xiaowei, "A Robust Asymmetric Kernel Function for Bayesian Optimization, with Application to Image Defect Detection in Manufacturing Systems," *IEEE Transactions on Automation Science and Engineering*, vol. 19, no. 4, 2021, pp. 3222–3233, IEEE.
- [18] Yin, Feng, Pan, Lishuo, Chen, Tianshi, Theodoridis, Sergios, Luo, Zhi-Quan Tom, and Zoubir, Abdelhak M., "Linear Multiple Low-Rank Kernel Based Stationary Gaussian Processes Regression for Time Series," *IEEE Transactions on Signal Processing*, vol. 68, 2020, pp. 5260–5275, IEEE.
- [19] H.C. Thacher, "New backward recurrences for Bessel functions," *Mathematics of Computation*, vol. 33, no. 146, pp. 744–764, 1979.
- [20] Y.L. Luke, *Integrals of Bessel Functions*. Courier Corporation, 2014.
- [21] E. Grosswald, *Bessel Polynomials*, vol. 698. Springer, 1978.
- [22] M. Carley, "Numerical solution of the modified Bessel equation," *IMA Journal of Numerical Analysis*, vol. 33, no. 3, pp. 1048–1062, 2013.
- [23] J. Butcher, "Runge-Kutta methods," *Scholarpedia*, vol. 2, no. 9, p. 3147, 2007.
- [24] Gramacy, Robert B. *Surrogates: Gaussian Process Modeling, Design, and Optimization for the Applied Sciences*. Chapman and Hall/CRC, 2020.
- [25] Nesi, Lucas Leandro, Arnaud Legrand, and Lucas Mello Schnorr. "Exploiting system-level heterogeneity to improve the performance of a geostatistics multi-phase task-based application." In *Proceedings of the 50th International Conference on Parallel Processing*, pp. 1–10, 2021.
- [26] The Chameleon project, "Chameleon: A dense linear algebra library for heterogeneous architectures," Dec. 2024. [Online]. Available: <https://project.inria.fr/chameleon/>
- [27] G. Bosilca, A. Bouteiller, A. Danalis, M. Faverge, A. Haidar, T. Herault, J. Kurzak, J. Langou, P. Lemarinier, H. Ltaief, et al., "Flexible development of dense linear algebra algorithms on massively parallel architectures with DPLASMA," in *2011 IEEE International Symposium on Parallel and Distributed Processing Workshops and PhD Forum*, IEEE, 2011, pp. 1432–1441.
- [28] C. Augonnet, S. Thibault, R. Namyst, and P. A. Wacrenier, "StarPU: a unified platform for task scheduling on heterogeneous multicore architectures," in *Euro-Par 2009 Parallel Processing: 15th International Euro-Par Conference, Delft, The Netherlands, August 25-28, 2009. Proceedings 15*, Springer, 2009, pp. 863–874.
- [29] R. Hoque, T. Herault, G. Bosilca, and J. Dongarra, "Dynamic task discovery in PARSEC: A data-flow task-based runtime," in *Proceedings of the 8th Workshop on Latest Advances in Scalable Algorithms for Large-Scale Systems*, 2017, pp. 1–8.
- [30] S. Abdulah, H. Ltaief, Y. Sun, M. G. Genton, and D. E. Keyes, "Parallel approximation of the maximum likelihood estimation for the prediction of large-scale geostatistics simulations," in *2018 IEEE International Conference on Cluster Computing (CLUSTER)*, IEEE, 2018, pp. 98–108.
- [31] S. Abdulah, H. Ltaief, Y. Sun, M. G. Genton, and D. E. Keyes, "Geostatistical modeling and prediction using mixed precision tile Cholesky factorization," in *Proceedings of the 2019 IEEE 26th International Conference on High Performance Computing, Data, and Analytics (HiPC)*, 2019, pp. 152–162.
- [32] Q. Cao, S. Abdulah, H. Ltaief, M. G. Genton, D. Keyes, and G. Bosilca, "Reducing data motion and energy consumption of geospatial modeling applications using automated precision conversion," in *2023 IEEE International Conference on Cluster Computing (CLUSTER)*, IEEE, 2023, pp. 330–342.
- [33] Plesner, A., Sørensen, H.H.B. and Hauberg, S., 2024, May. Accurate Computation of the Logarithm of Modified Bessel Functions on GPUs. In *Proceedings of the 38th ACM International Conference on Supercomputing* (pp. 213-224).
- [34] J. B. Campbell, "On Temme's Algorithm for the Modified Bessel Function of the Third Kind," *ACM Transactions on Mathematical Software*, vol. 6, no. 4, pp. 581–586, Dec. 1980.

- [35] Watson, G. N. (1922). *A treatise on the theory of Bessel functions* (Vol. 2). The University Press.
- [36] Paul, C. Abbott. *Mathematica*. In *Revival: The Handbook of Software for Engineers and Scientists (1995)*, pages 926–962. CRC Press, 2018.
- [37] Salvaña, Mary Lai O., Sameh Abdulah, Hatem Ltaief, Ying Sun, Marc G. Genton, and David E. Keyes. "Parallel space-time likelihood optimization for air pollution prediction on large-scale systems." *Proceedings of the Platform for Advanced Scientific Computing Conference*, 2022, pp. 1–11.
- [38] Sun, Ying, and Michael L. Stein. "Statistically and computationally efficient estimating equations for large spatial datasets." *Journal of Computational and Graphical Statistics*, vol. 25, no. 1, 2016, pp. 187–208. Taylor & Francis.